Eidgenössische Technische Hochschule Zürich
Swiss Federal Institute of Technology Zurich

SED
Schweizerischer Erdbebendienst
Swiss Seismological Service

Report on site characterization

Lenzkirch, Germany (BERGE)

Poggi Valerio, Ulrike Kleinbrod, Donat Fäh

Last modified - 24 / 12 / 2014

1. Introduction

In the framework of the NAGRA seismic network project, an array measurement of the ambient vibration wave-field was performed at the location of the SED station BERGE (Lenzkirch, Germany). The scope of the survey is the seismic characterization of the area surrounding the installation (**Figure 1**), which consists in a broadband seismometer (Trillium Compact) with a high-resolution digitizer (Taurus 24Bit @200sps). Ambient vibration analysis has been used to infer the characteristics of the underground structure of the site, with special regard to the one-dimensional shear-wave velocity. Such profile was later used to assess the local seismic response of the station.

For the analysis, different spectral analysis techniques were implemented, consisting in both single and array methods, which are listed below:

- Time-frequency wavelet analysis
- Power-spectral density estimation
- Conventional horizontal to vertical spectral ratios
- Directional horizontal to vertical spectral ratios
- Wavelet polarization analysis
- Three-component high-resolution f-k analysis.

The results of all these analyses conformed to the definition of the final velocity model. In the following, the main results of these investigations are summarized and a final interpretation of the velocity profile is given. From this interpretation, engineering parameters are finally derived, e.g. the Qwl-Vs average velocity, VsZ (including Vs30) and the seismic amplification from the analytical SH-transfer function of the one-dimensional soil column.

2. Survey description

To characterize the seismic response of the site, a first array measurement of ambient vibration was performed on 22/03/2013. This array consisted in two measuring configurations of 14 sensors each and increasing diameters of 100m and 200m respectively. The two configurations were planned to partially overlap, by sharing 9 common sensors, with the aim of providing a continuous resolution of the frequency range between the two geometries. Unfortunately, the first experiment was unsuccessful, mostly due to unfavorable survey conditions (**Figure 2**A); the acquisition was performed one day after a moderate snowfall, during the melting phase of the snow cover. This created considerable side problems: soil saturation, disturbances induced by the underground water flow and bad coupling/tilting of the sensors at the surface. No results were then obtained from these recordings, as no evidence of coherency of the ambient vibration wave-field was present in the resolvable frequency band (**Figure 3**A).

The survey was then repeated (19/06/2013), with better weather and soil conditions (**Figure 2**B). For this second measurement, given the acquired information about the possible subsurface geology of the area (see following section), it was decided not to implement the small configuration anymore, but to only perform the large geometry of 200m in size (**Figure 1**). This decision was taken on the base of the expected very high phase-velocities of the surface waves for hard rock sites (mostly gneiss and high-grade metamorphic units), which usually require larger array to be successful. A prior estimation of the possible maximum penetration depth was however not possible in this case, due to the large uncertainty of the bedrock velocity.

During the survey, a total of about two hours of recordings has been acquired. By band-pass filtering, the presence of coherency in the ambient vibration wave-field is now evident (**Figure 3**B). However, not all the stations recorded properly for the entire time. One station stopped working unexpectedly due to a failure of the battery; one station had GPS synchronization problems at the beginning; the baler of one station did not properly flush data, leading to a loss of about 20min of recordings. To face these problems and in order to achieve the best compromise between available stations and recording length, two different processing sub-configurations have been tested (**Figure 4**). The configuration named "*Selection 1*" was nevertheless the most successful in term of f-k resolution; the results in the following sections are then based on that geometry.

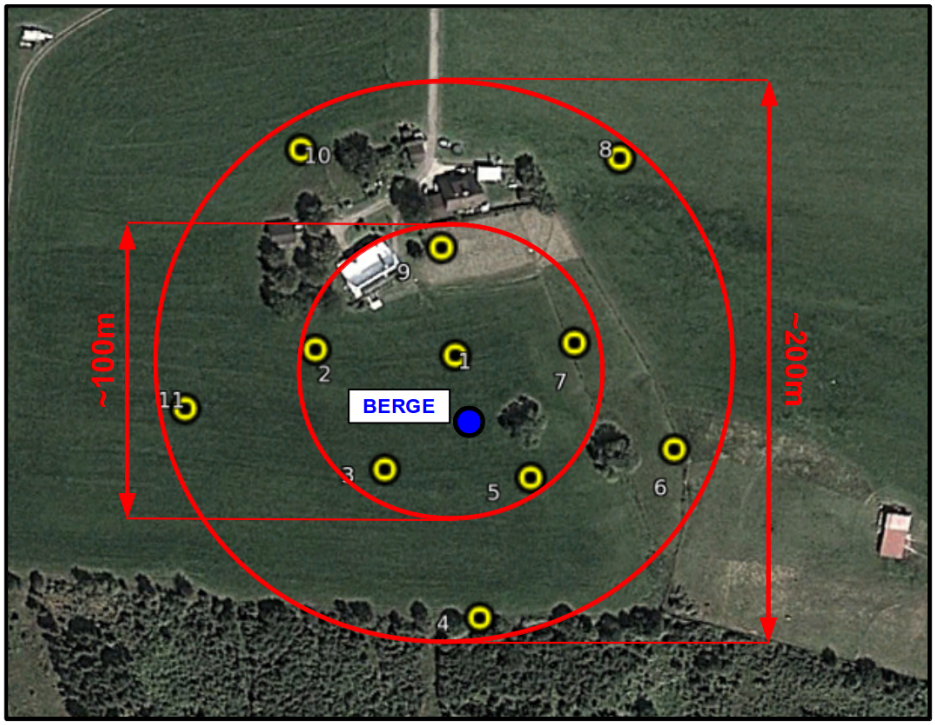

Figure 1 - *Geometry of the second ambient vibration array survey performed in Lenzkirch (SED station BERGE) on 19/06/2013. Two concentric rings of increasing diameter were used. The location of the seismic station is shown in blue.*

A)

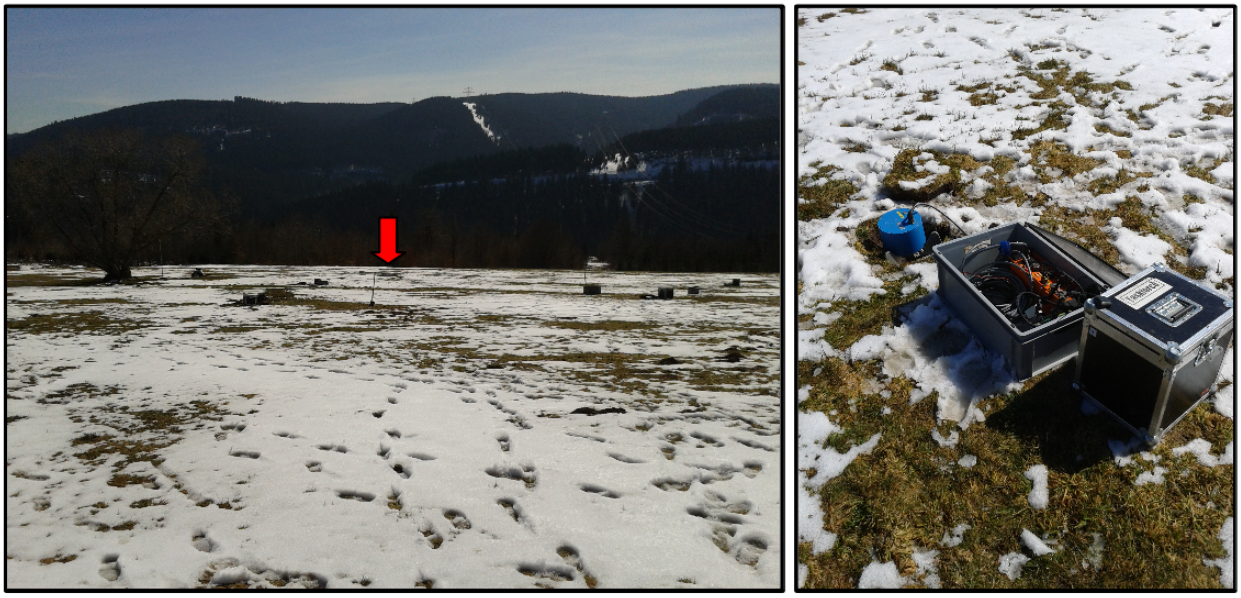

B)

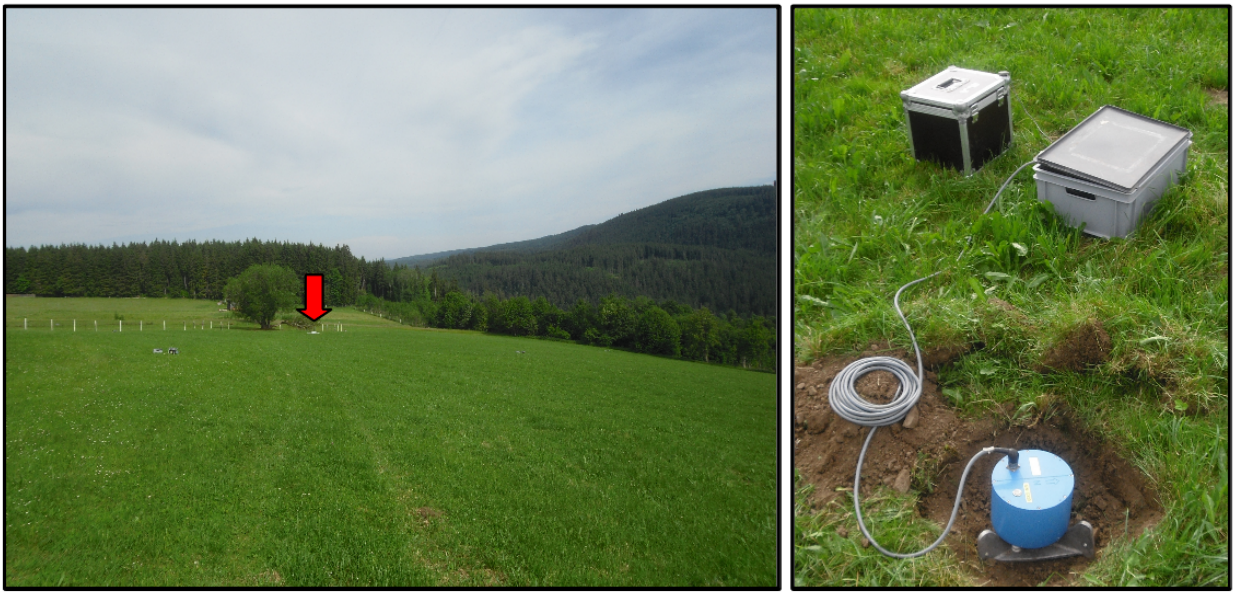

Figure 2 - *Comparison of the general measuring conditions between the two experiments performed respectively in March (A) and June (B) 2013. The red arrow indicates the location of the SED station installation. On the right side, details of single acquisition points of the array, consisting of a Q330 datalogger (in the gray box) and a Lennartz 5s velocity seismometer. The coupling of the sensor is assured by removing the uppermost part of the soil and by means of a special support (Trihedron).*

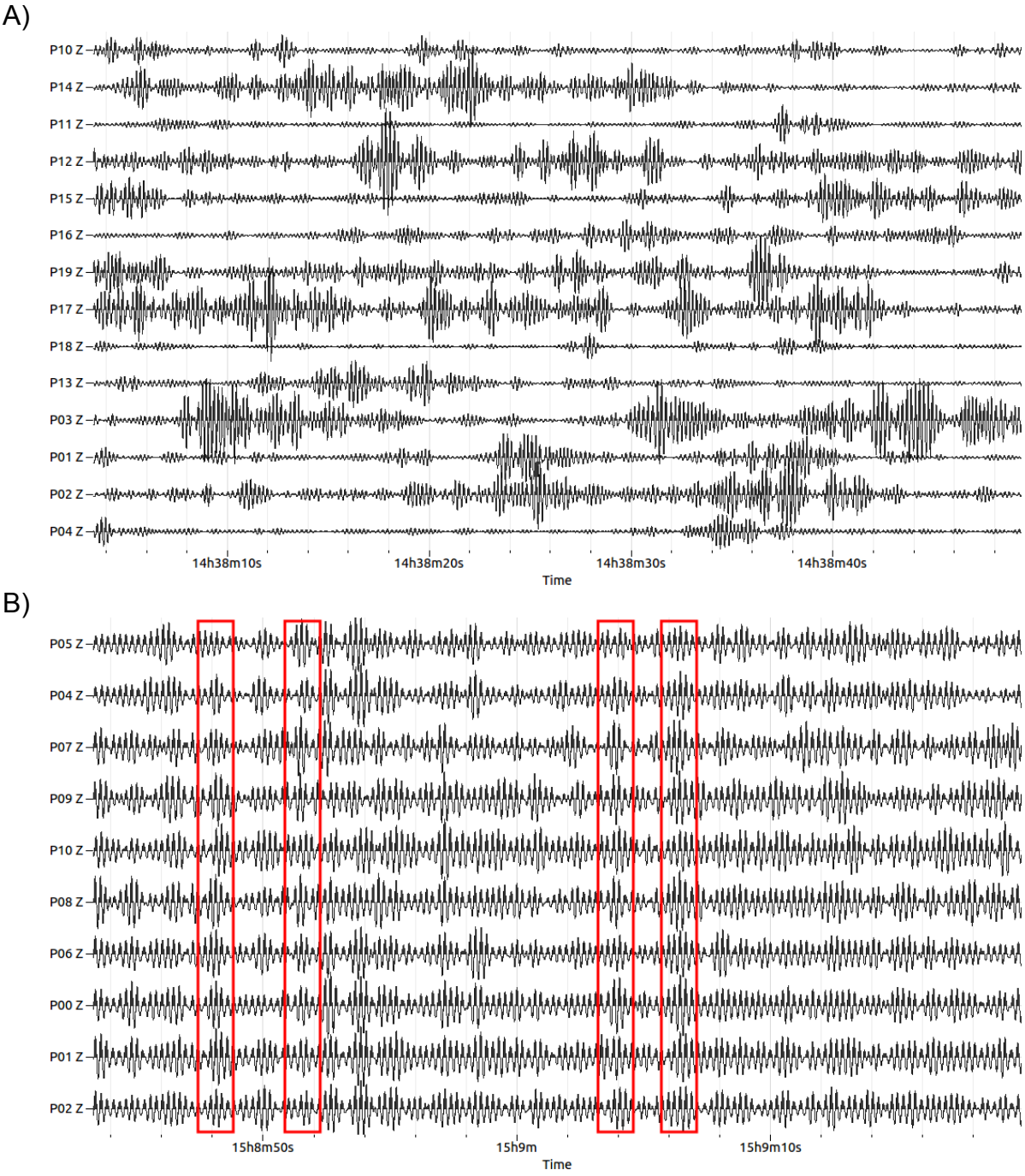

Figure 3 - *Comparison between the recordings from the two surveys performed in March (A) and June (B) 2013 at the station BERGE. For better comparison, the signal's windows are of the same duration and band-pass filtering (4-6Hz, 6th order causal Butterworth). The wave-field in A did not show any sign of coherency, while it is evident in B the presence of numerous correlated signals (e.g. marked with red boxes).*

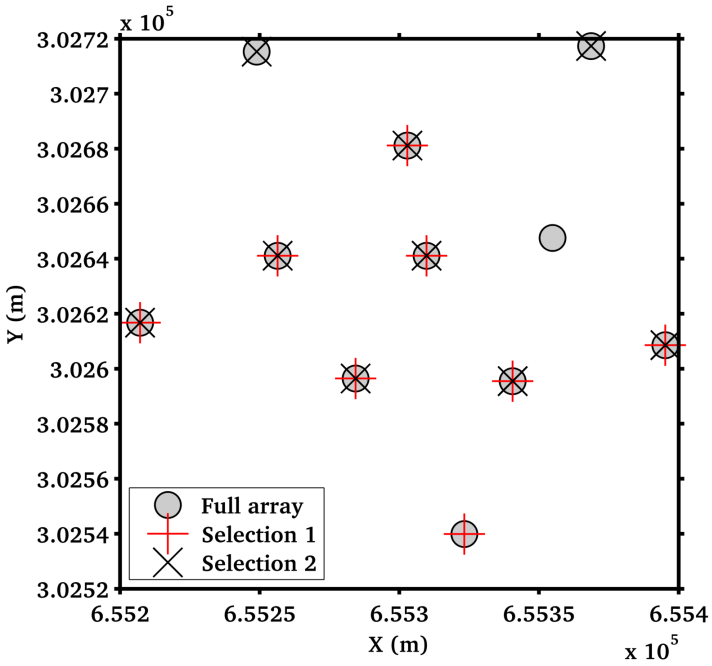

Figure 4 - *Geometry of the two sub-selections obtained from the full array performed on March 2013 in Lenzkirch. Selection 1 consisted of eight stations and about 1h10m of recordings, while for the selection 2 nine stations were included with 40m recording duration.*

3. Soil type, topography and geology

The array has been set in open field conditions, in a rural area (**Figure 1**, **Figure 2**). The influence of buildings and anthropogenic disturbances is virtually negligible. Sensors have been deployed on free soil conditions. Good coupling with the ground was assured by means of digging small holes at the sensor's places, and by using a special support (*Trihedron*) that facilitates the leveling of the device even for difficult soil conditions. The measurement area is located on a moderate slope dipping toward south. However, no topographic correction has been taken into account before processing.

From the geological points of view (**Figure 5**), the target area is located within the Feldberg massif, a relevant geological unit of the Black Forest area. It mostly consists in granite and gneiss of different metamorphic degree. The bedrock is very shallow at the measuring location, but never exposed across the area. The surface morphology is considerably smooth and modeled by the action of glaciers during the Pleistocene. Such site can be classified as of rock ground-type A.

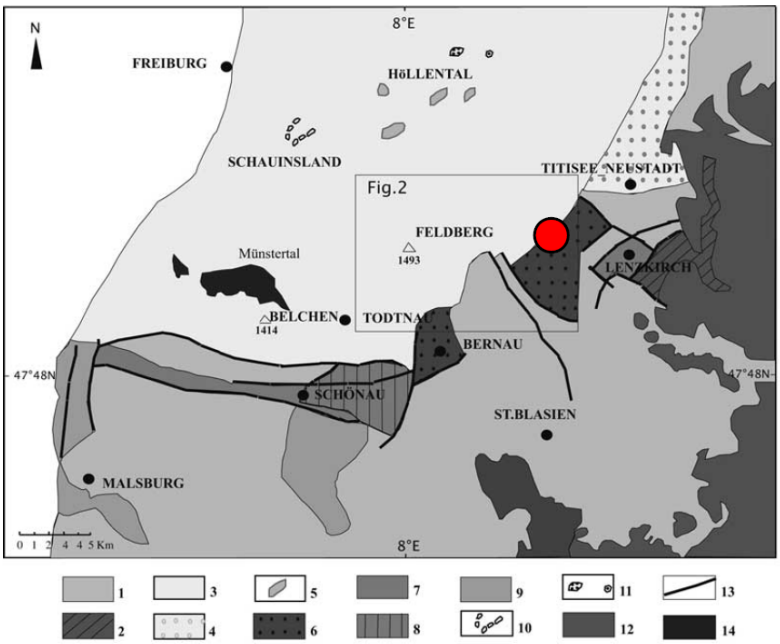

1: granite;
2: rhyolite;
3: gneiss;
4: gneiss with quartzite;
5: orthogneiss;
6: other metamorphic units;
7: Palaeozoic sediments;
8: metamorphosed greywackes;
9: blastites;
10: calcareous silicate rock;
11: Permian sediments;
12: Triassic sandstones;
13: fault;
14: Permian rhyolites.

Figure 5 - *Simplified geological map of the Feldberg massive area (from Huguet 2007, modified). In red the approximate location of the array measurement in Lenzkirch is marked.*

4. Acquisition equipment

Each acquisition point within the array consisted of a three components seismometer (Lennartz 3C with 5s eigenperiod, **Figure 2**) and a 24 bit data logger (Quanterra Q330). Synchronization between stations was assured by standard GPS, while a more accurate differential GPS (Leica Viva system) was used to precisely locate the sensor's coordinates with a tolerance of less than 5cm.

5. Weather conditions

The first measurement (22/03/2013) was performed one day after a moderate snowfall. The average temperature was however above zero at around noon, which caused the partial melt of the snow cover. The ground was consequently saturated with water during the acquisition, which caused coupling/tilting problems to the sensors and the generation of considerable local (uncorrelated) noise disturbances. Conversely, the weather conditions were stable during the second measurement (19/06/2013), with no precipitations and an average (over the whole day) temperature of 25 degrees.

6. Pre-processing and preliminary data-quality control

The three-component recording has been preliminary band-pass filtered using a high-pass 6th order causal Butterworth filter in the bands 0.2-1Hz, 1-4Hz, 4-6Hz and 6-10Hz. Although it is not a requirement for spectral analysis techniques, such filtering was applied in order to facilitate the preliminary visual inspection of the noise traces (e.g. **Figure 3**) and to evaluate the coherency of the wave-field in the different frequency bands. Such procedure gives essential information for the subsequent interpretation of the f-k analysis results.

To assess the quality of the ambient vibration recordings, spectral analysis was subsequently performed. Because of the stochastic nature of the ambient vibration wave-field, a statistical approach has to be used, such as the estimation of the power spectral density (*PSD*). This approach is useful to evaluate the average energy level of the recordings in the analyzed frequency range, and to access the presence of spurious spectral peaks, which might be related to human activity (machinery, pumps). By inspecting the PSD of the three-component recordings at the central station in the range between 0.5 and 40Hz (e.g. **Figure 6**, separately for the three components), only one spurious peak is visible at about 4.2Hz, but more pronounced on the vertical direction. The peak - very narrow - is most likely of anthropogenic origin (from the nearby farm) and should be rejected from interpretation. The average energy level is nevertheless very low, close to the minimum bound of the USGS noise model.

Complementary to the aforementioned statistical methods, a spectral decomposition approach is more suitable to assess the stationarity of the ambient vibration wave-field over time. The wavelet time-frequency analysis was then performed over the whole recording time. From such analysis (**Figure 7**) an overall stability of the ambient-vibration wave-field over time is evident. The disturbance at 4.2Hz is confirmed to be a nearly harmonic contribution, steady over the whole recording window. This provides an additional confirmation of its possible anthropogenic origin. The disturbance is nevertheless very weak and well localized in frequency; therefore it won't affect the following processing steps.

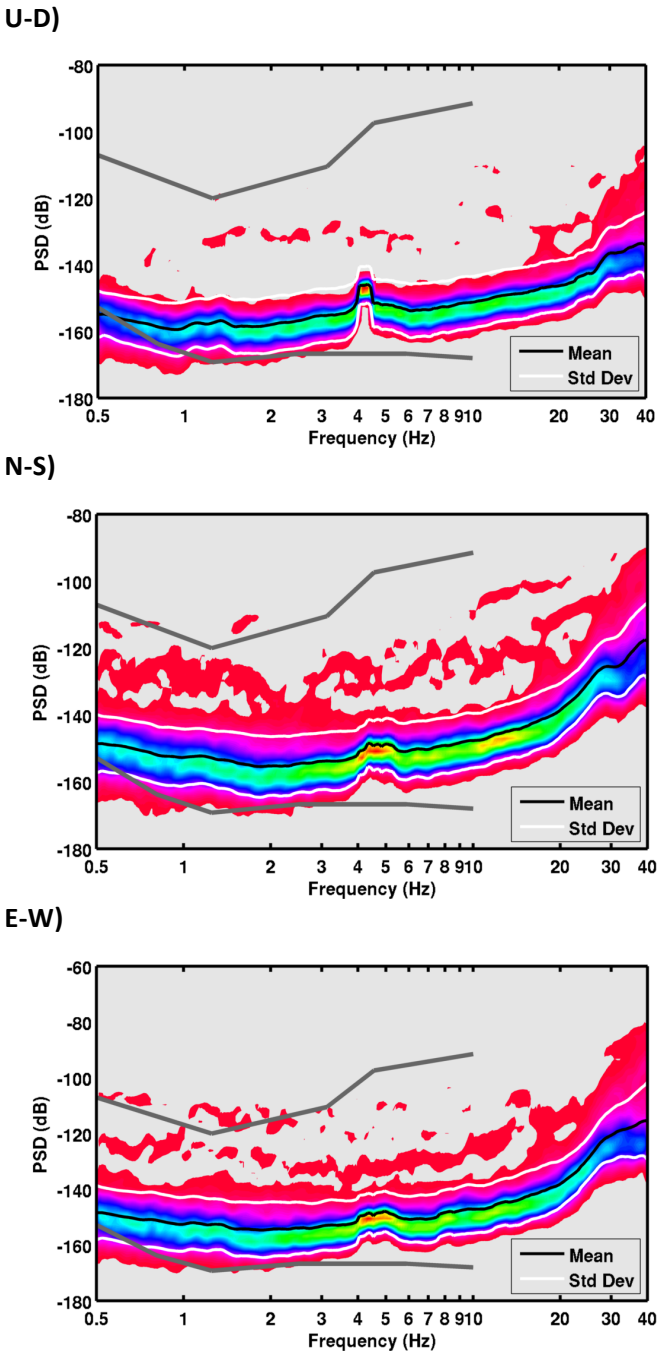

Figure 6 - *Power spectral density (PSD) computed for 1h10m recording at the central station of the array (point P0). Similar results were obtained from the other stations of the array. In gray lines are the minimum and the maximum bounds of the USGS noise model, for comparison.*

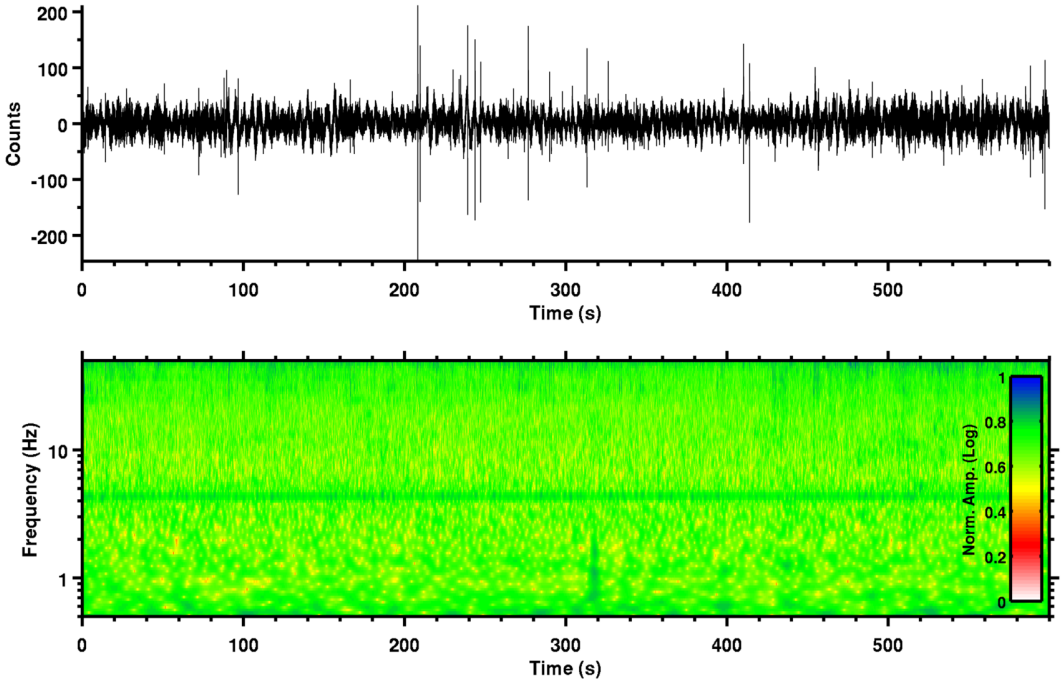

Figure 7 - *Example of spectrogram from 600s of recording of the central station of the array (P0, vertical component). For the analysis, the cosine wavelet is used (wavelet parameter = 12). It is visible on the whole spectrogram the harmonic disturbance at about 4.2Hz, which is nevertheless not particularly energetic.*

7. Conventional H/V spectral ratios

The horizontal-to-vertical (H/V) Fourier spectral ratio is a technique widely used in seismic site characterization because of its ability to provide an estimate of the SH wave fundamental frequency of resonance (f_0) of the site. Other than that, H/V ratios are useful to provide information on the Rayleigh wave ellipticity function, which can be used in the inversion procedure to constrain large velocity contrasts at depth. In this study, we use the H/V technique also to map the variability of the subsoil structure along the investigated area; this is necessary to verify the fulfillment of the 1D structure assumption, which is necessary for the f-k method applied later.

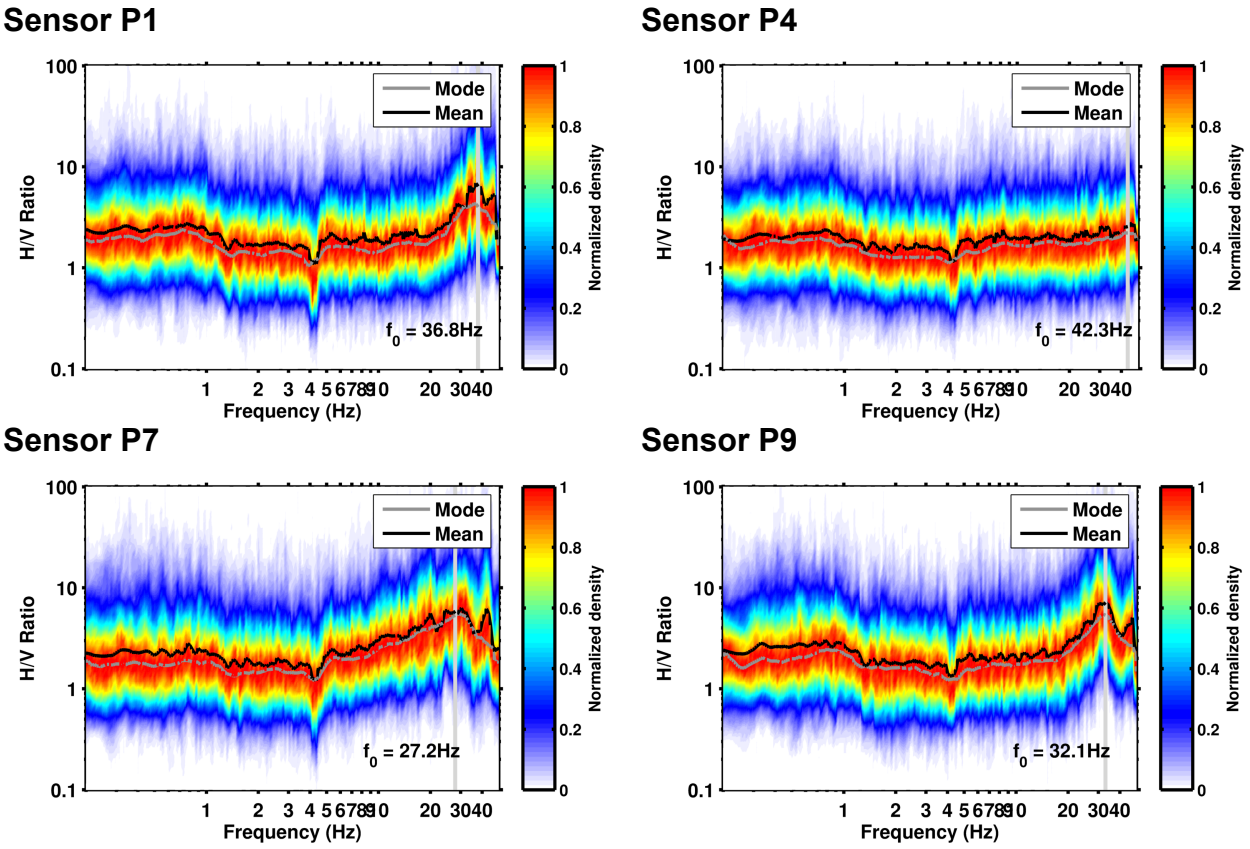

Figure 8 - *Example of H/V spectral ratios at four stations of the array (Selection 1). The resonance frequency of the soil cover is indicated with a light gray line (between 25~50Hz).*

H/V spectral ratios have been computed for the recordings at each station of the array (e.g. **Figure 8**). The behavior of the noise wave-field at the different stations location is comparable (**Figure 9**). A weak maximum on the H/V curves is present at about 0.8Hz, and might be addressed as the resonance frequency of the sites due to a velocity contrast in the rock profile. The peak is very stable over the array, but very low in amplitude. Considering the characteristic of a generic rock site, such maximum might be induced by a change in lithology within the profile at depth, which causes a moderate contrast of seismic impedance. The effect of the topmost soil cover is visible at high frequencies (> 20Hz), where large amplitude resonance peaks are noticeable. The peaks are nevertheless not comparable across the array (in amplitude and frequency), as confirmation of the heterogeneity of the very thin soil cover. The behavior of the site can be considered laterally homogeneous for the f-k analysis.

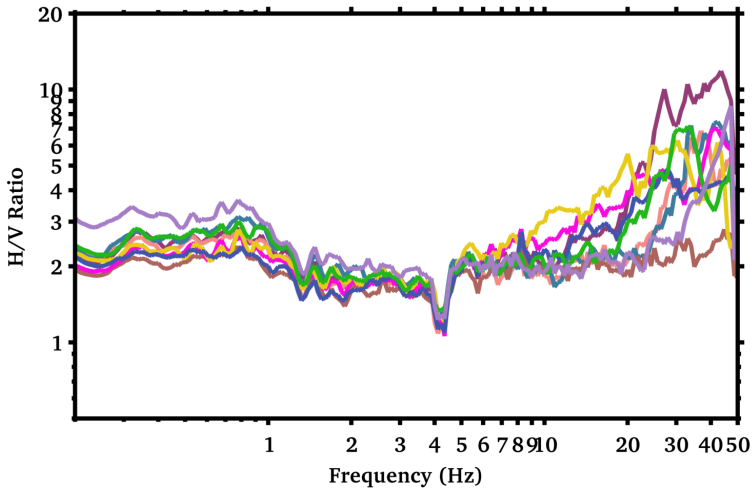

Figure 9 - *Comparison of the H/V spectral ratio curves of all the stations of the array (Selection 1). The curves are stable up to at least 20Hz, confirming the lateral homogeneity of the velocity structure of the site. A low frequency peak is visible at about 0.8Hz, which might be considered the fundamental frequency of the site.*

8. Directional H/V spectral ratios

The computation of directional H/V spectral ratio or polarization analysis is useful to reveal asymmetries in the ambient vibration wave-field. Different effects can induce such a behavior: 2D/3D structure, topographic effects or a non-homogeneous distribution of the noise sources. If a strong directionality is found by the analysis, it is generally recommended to carry out further investigations to properly address the origin of polarization.

By processing the directional H/Vs at all the recording stations of the array (e.g. **Figure 10**) it is possible to observe an isotropy of the wave-field in the low frequency range, roughly below 20Hz. At high frequencies, however, the variability of the H/V peak is noticeable also in their directionality. This can be explained by the variability of the uppermost soil cover layer over the study area, and it cannot be interpreted as an effect of non-homogenous distribution of the noise sources. This issue is later investigated through f-k analysis. The topographic slope seems to have no effect on the ambient vibration wave-field.

The result of the directional analysis is also confirmed by applying the wavelet polarization analysis techniques as described in Burjanek et al. (2008) to the central station of the array. Also in this case no significant directionality (**Figure 11**a) and polarization (**Figure 11**b) of the wave-field are observable.

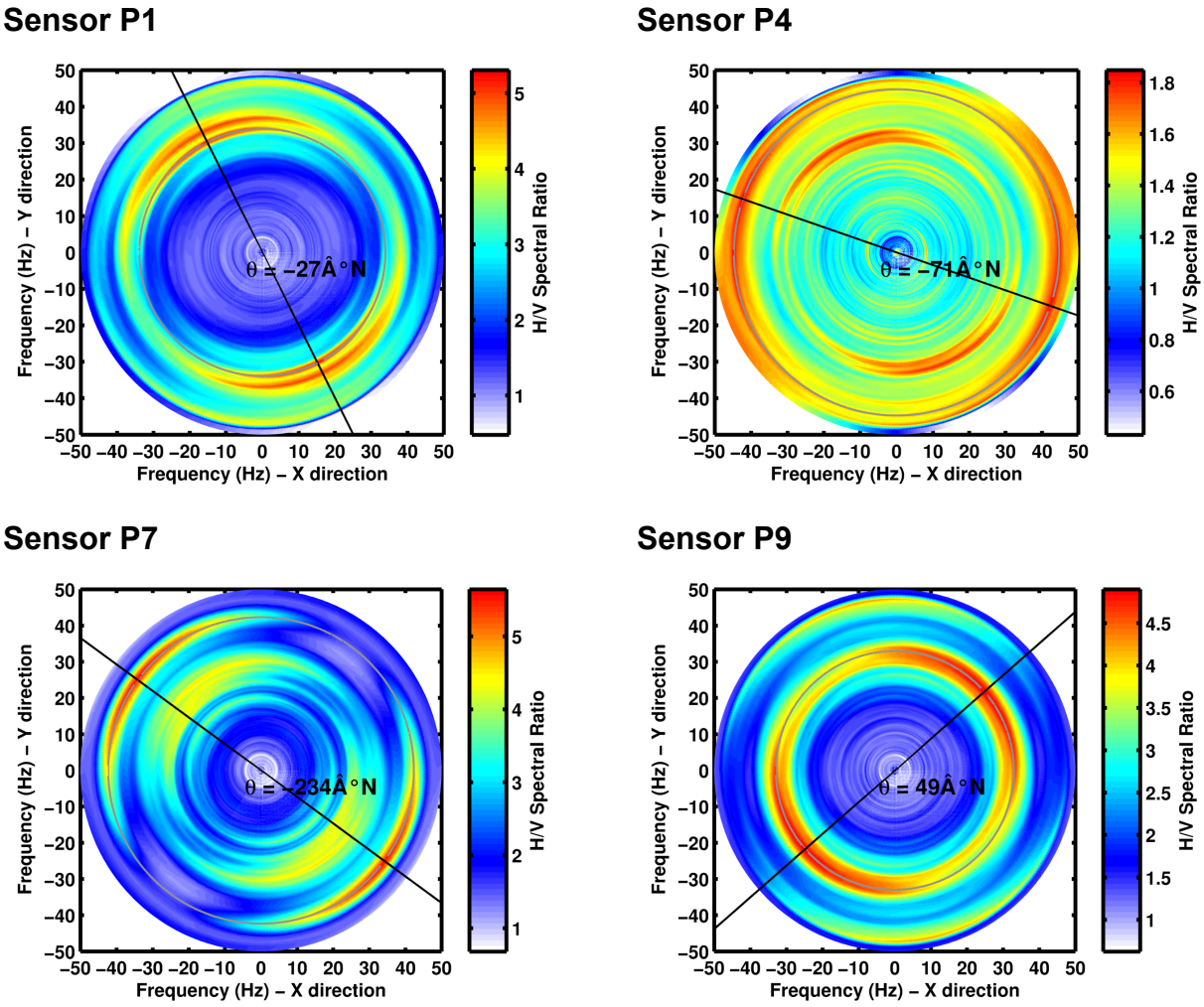

Figure 10 - *Example of directional H/V spectral ratios at four stations of the array configuration A. No consistent evidence of wave-field anisotropy is present below 20Hz.*

a)

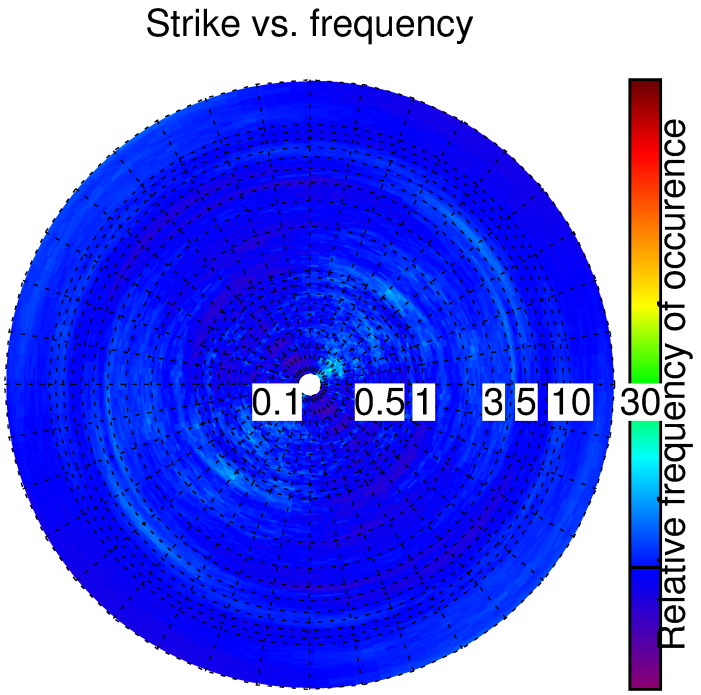

b)

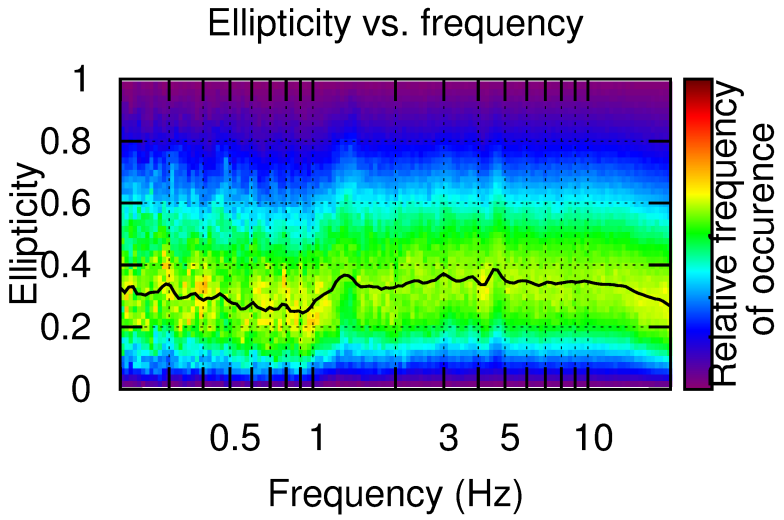

Figure 11 - *Wavelet-based polarization analysis at the central station of the array. By analyzing the polarization over strike (a) and the particle motion ellipticity plot (b), no directional effect is visible in the frequency range of interest.*

9. Three-component f-k analysis

The frequency-wavenumber analysis is a spectral technique based on seismic array recordings that allows retrieving the direction and the dispersion characteristics of the surface waves. We apply here this technique to three-component ambient vibration recordings using a modification of the high-resolution method of Capon (1969) as described in Poggi et al. (2010). Using all the three-components of motion gives the possibility to retrieve information about the propagation of the Rayleigh waves (vertical and radial processing direction) as well as of the Love waves (transversal direction).

As in the case of the previous methods, the ambient vibration recordings are treated statistically by subdividing the traces in sub-windows. For each consecutive window a separated f-k analysis is performed, and the results are then averaged over the whole recording, increasing the robustness of the final estimation.

a) 6-10Hz Hz

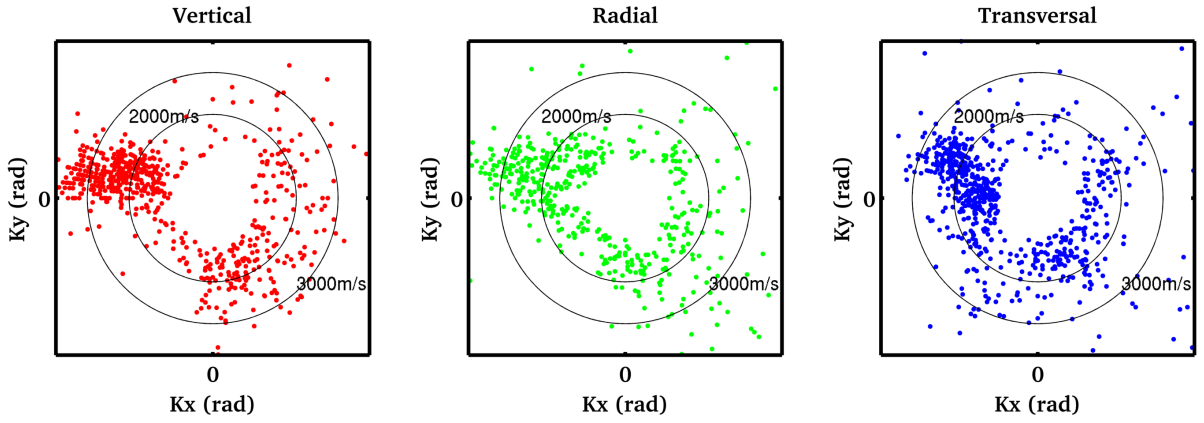

b) 15-20 Hz

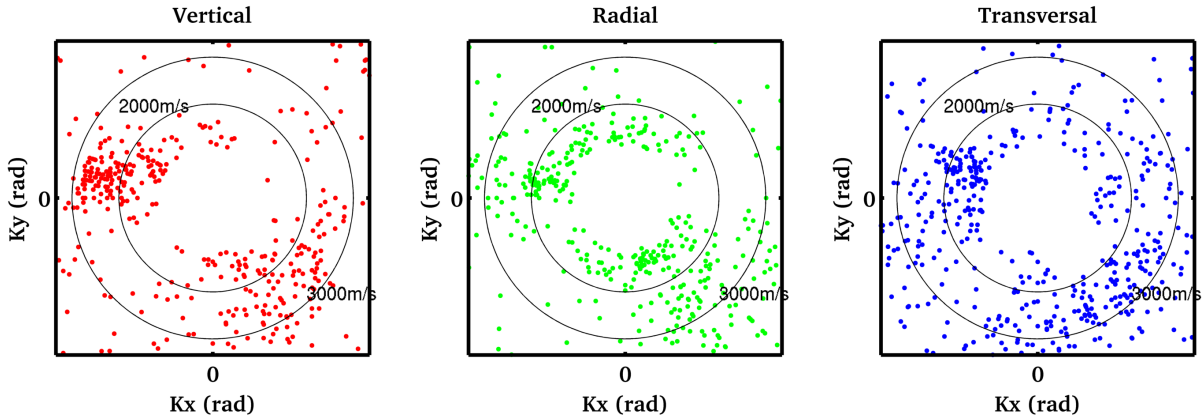

Figure 12 - *Example of distribution of noise sources in the intermediate frequency range (6-10Hz) and at high frequencies (15-20Hz), obtained from three-components f-k analysis (Station selection 1).*

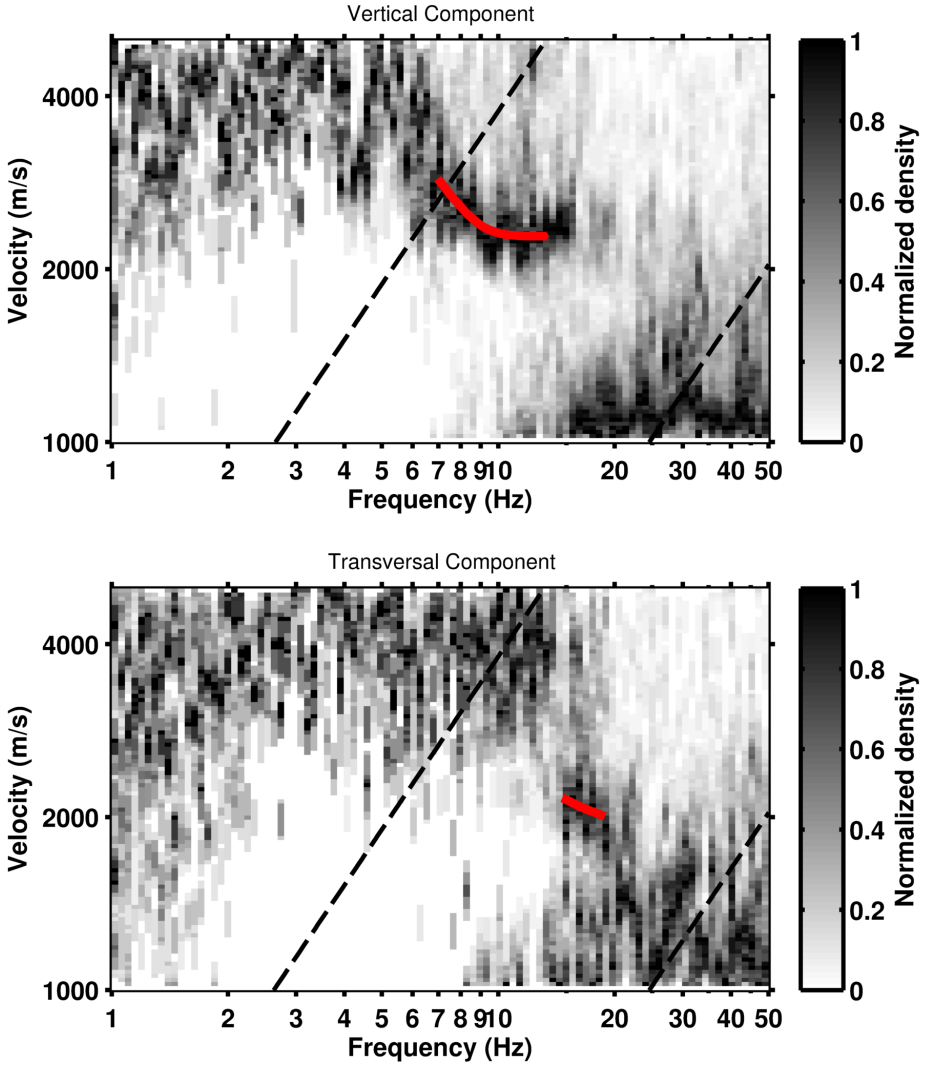

Figure 13 - *Density distribution of all the surface wave signals obtained from the whole recording of the BERGE array (Selection 1) using f-k analysis. Top: result from the analysis of the vertical component (Rayleigh waves); Bottom: result for the transverse component (Love waves). In red the interpreted dispersion curves are given (manually selected).*

As first step, from the f-k analysis it was possible to assess the noise source distribution over broad range of analyzed frequencies (e.g. **Figure 12**) for the vertical, the radial and the transversal component. In particular, in the intermediate frequency range (6-10Hz) the source distribution show a remarkable cluster in NWW direction on all the components. This is not surprising, because this direction is consistent with the location of the farmer house with respect to the array; this is probably the strongest source of noise in the area.

Subsequently, the surface-wave dispersion curves have been extracted by visual inspection and manual picking of the f-k density plots (**Figure 13**). The Rayleigh wave dispersion can be tracked between about 6 and 14Hz, while for Love waves only a limited frequency band has sufficient energy for an interpretation. The phase velocities are in both cases very high, as expected for hard metamorphic rock. The final interpretation of the modal dispersion pattern is then presented in **Figure 14** for both the Rayleigh and Love waves, for comparison.

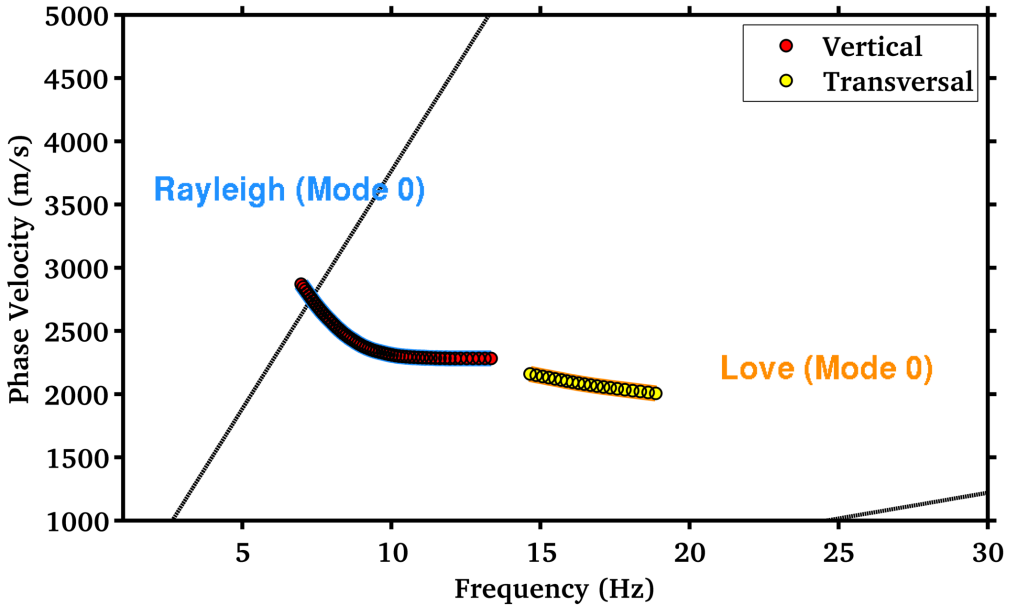

Figure 14 - *Final interpretation of the Rayleigh and Love dispersion curves from the station selection 1 of the BERGE array.*

10. Inversion of the dispersion curves

The surface wave dispersion curves (Rayleigh and Love) obtained from the three-component f-k analysis of the ambient vibrations were inverted to obtain an estimation of the velocity profile of the site (mainly S-wave velocity as function of depth, and to a lesser extend the P-wave velocity, due to the lower sensitivity). The analysis was performed using the software *Dinver* (www.geopsy.org), which implements a direct search approach (**Figure 15**) based on a conditional version of the neighborhood algorithm (Sambridge, 1999).

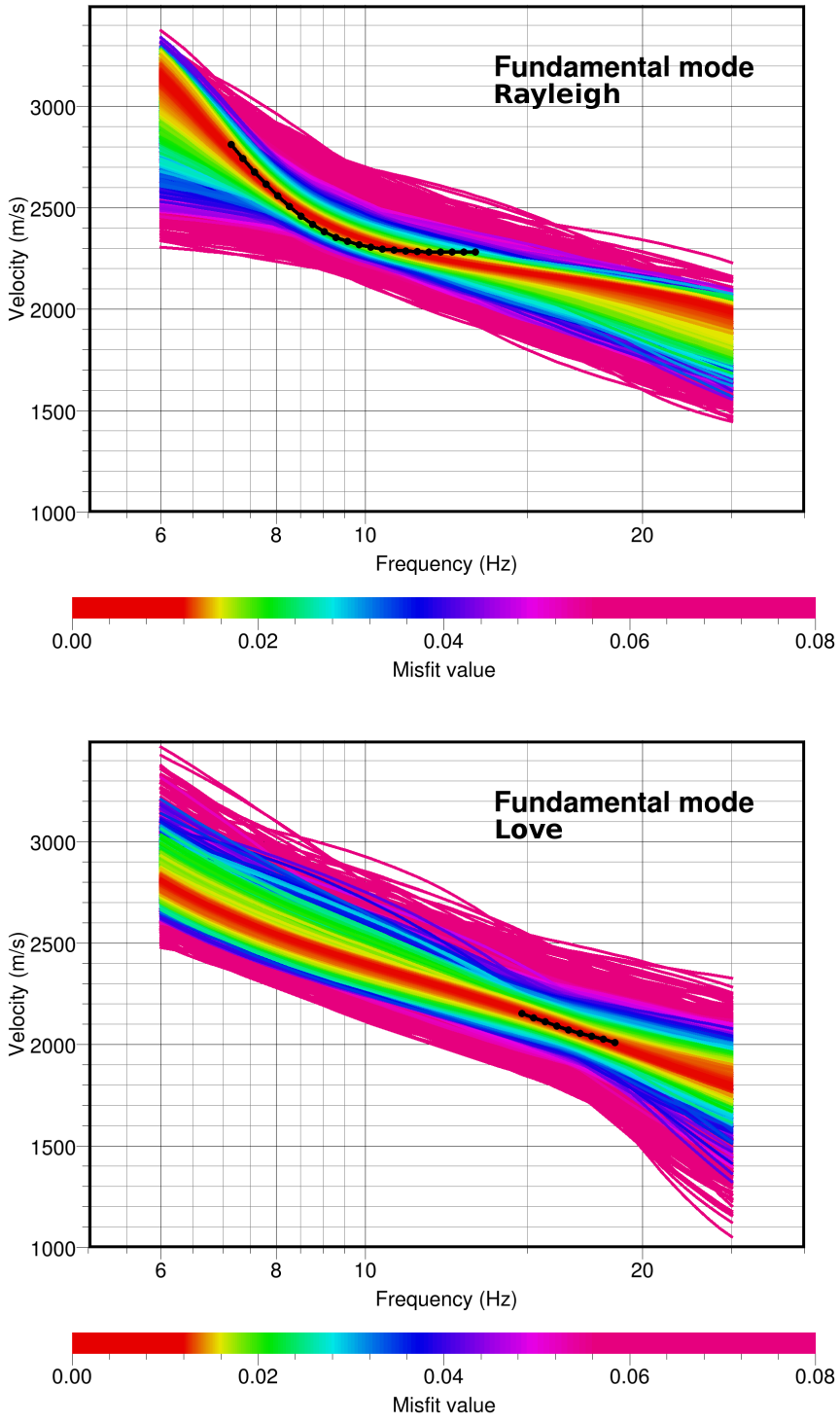

Figure 15 - *Fitting the surface dispersion data within the global optimization procedure. Different colors represent different misfit between the observed (in black) and the modeled dispersion curves during the search.*

To parameterize the velocity model, two different approaches were implemented. The first one consisted in setting up an eight-layer model with free interface depths (**Figure 16**). In such a case the free inversion parameters are then the velocities (P and S) and layer thicknesses. In the second case, a fixed-thickness layer approach was used (**Figure 17**). The advantage of the former method stays in the possibility to better resolve sharp velocity interfaces, while the second is less unique and better constraints the seismic velocity. The two approaches have to be nevertheless considered complementary, and they should provide consistent results.

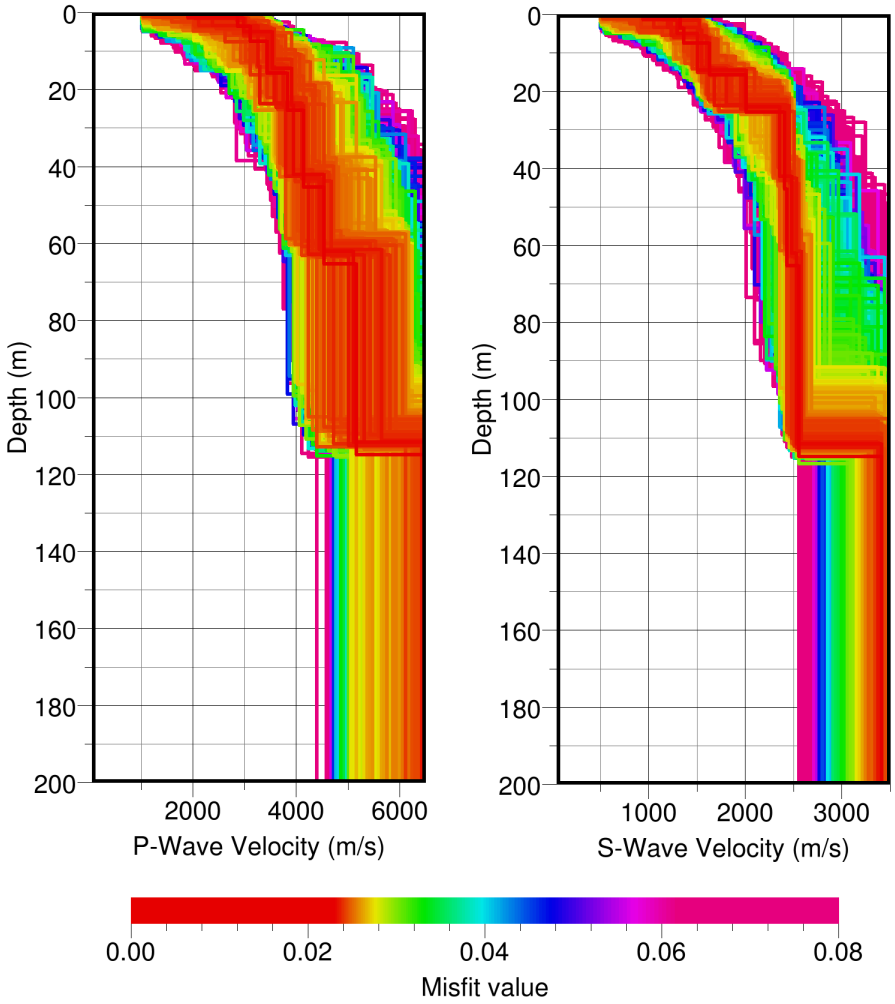

Figure 16 - *Distribution of the free-layer velocity models generated during the inversion process and ordered by decreasing misfit, according to the color scheme of* **Figure 15**.

Eight inversion tests (*runs*) have been performed for each of the two model schemes (**Figure 18**), in order to minimize the effect related to a possible unfavorable initial randomization of the space parameter. The best fitting models from of each run are then collected and used later on for the computation of the derived soil parameters.

The inverted velocity models (Vs and Vp) are gradient-like, with a faster increase in velocity in the first 10m, followed by a more smoothed part. This is expected for a rock velocity profile. By considering the minimum available frequency of the surface-wave dispersion curves, and by analyzing the scattering of the inverted models (**Figure 19**), it is realistic to assume the velocity profiles to be reliable down to a depth of about 80~100m. Below this value no direct constrain is available, and the velocity are obtained by pure extrapolation.

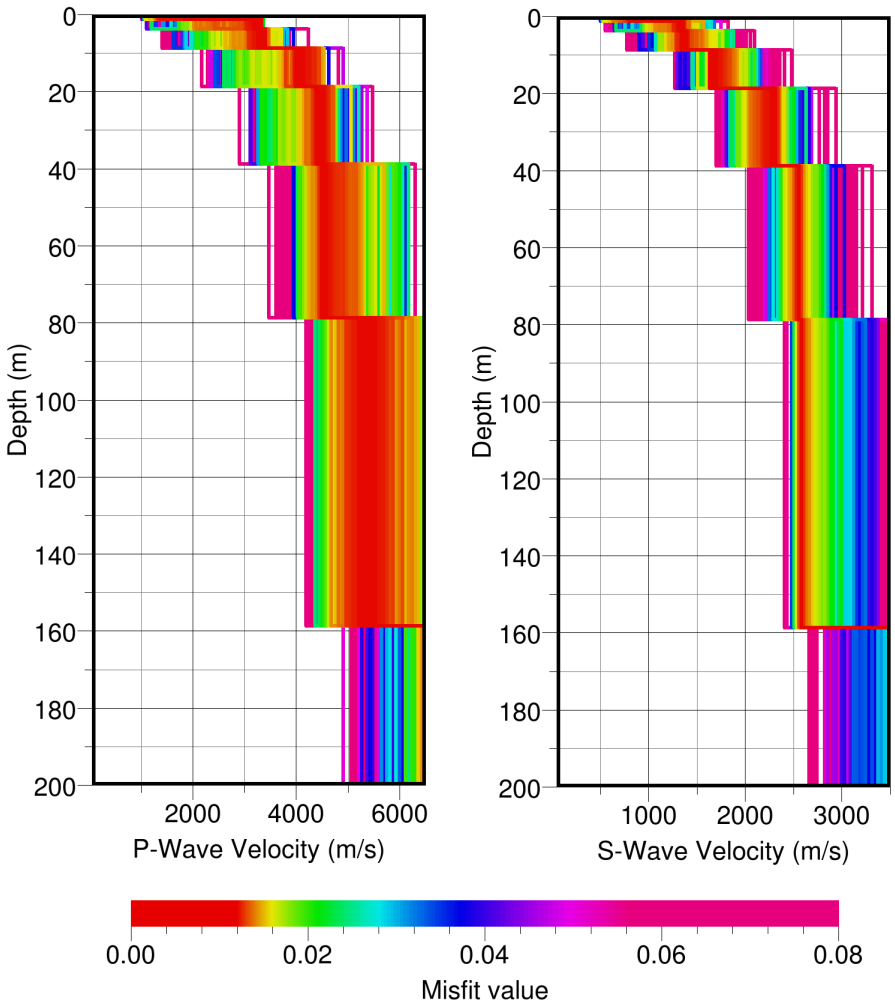

Figure 17 - *Distribution of the fix-layer velocity models generated during the inversion process, and ordered by decreasing misfit according to the color scheme of* **Figure 15**.

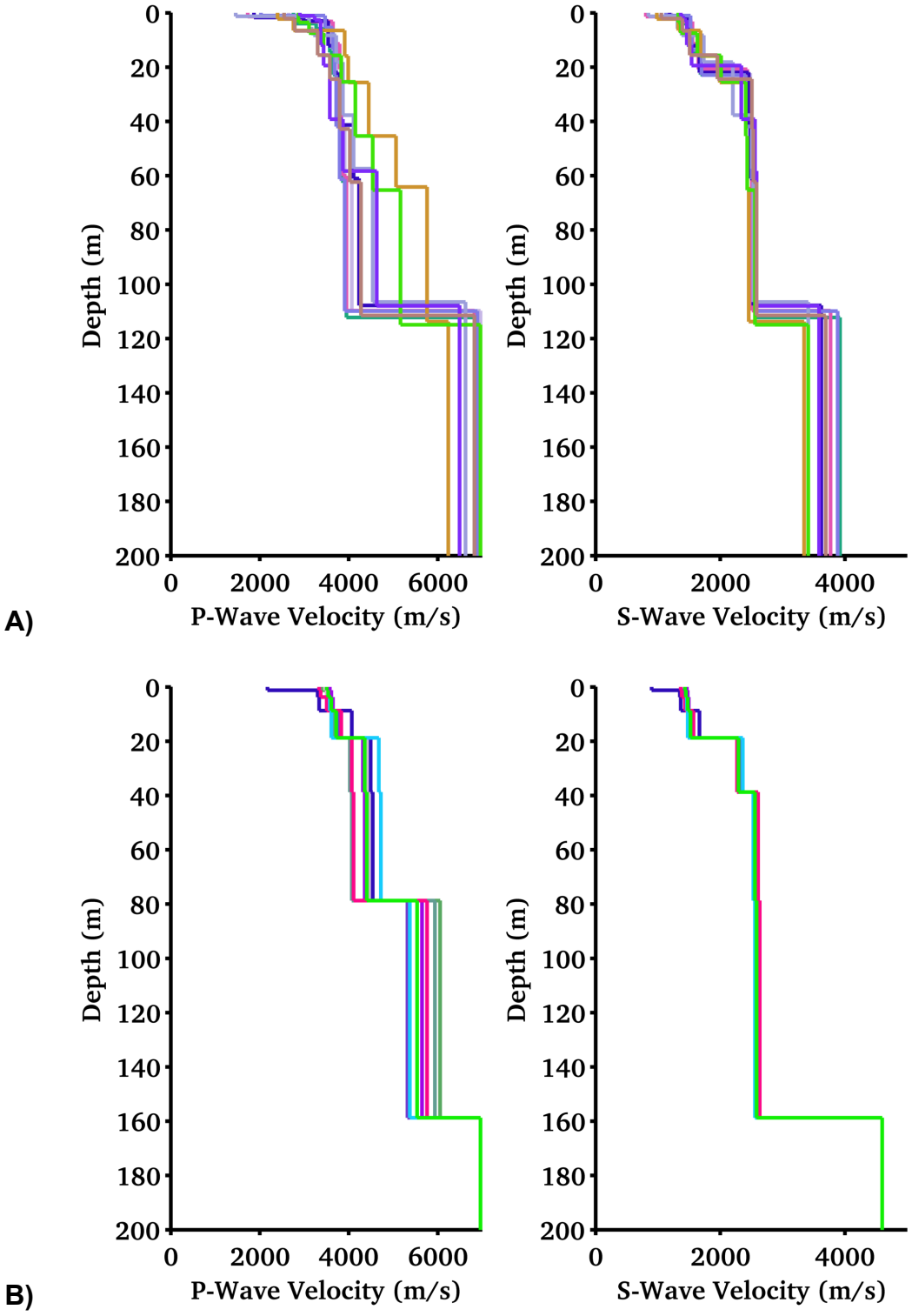

Figure 18 - *Collecting the best fitting models from the eight separated inversion runs using the free-layers (A, top) and fixed-layers (B, bottom) parameterization schemes.*

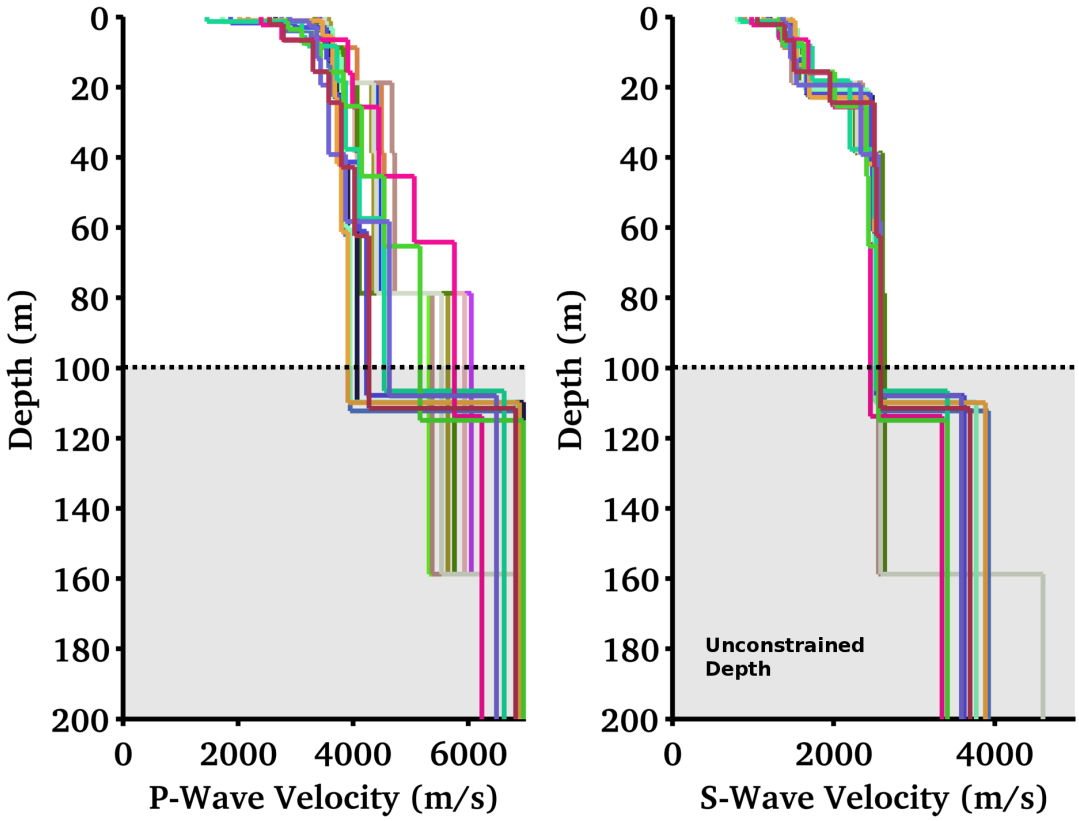

Figure 19 - *Comparison of all the best models from the two parameterization schemes (free and fixed layers). The two approaches are consistent down to a depth of about ~100m, which can be considered the maximum resolved depth.*

11. Engineering soil parameters

The ensemble of all the best inverted velocity profiles is then used to derive average soil parameters like the VsZ (average travel-time S-wave velocity over the depth Z, including Vs30, Table 1) and the quarter-wavelength (QWL) average velocities (Joyner et al., 1984) for a range of frequencies between 1 and 30Hz (**Figure 20**). The former is a standard parameter for the classification of ground-types in most building codes and in ground motion prediction equations. The latter is a parameter useful for the empirical estimation of the site-response and to assess the sensitivity of the seismic wave-field to the different depths. It has to be noticed that these two parameters are derived separately from all the best S-wave velocity models obtained from the inversion, and the results is finally averaged to improve statistics.

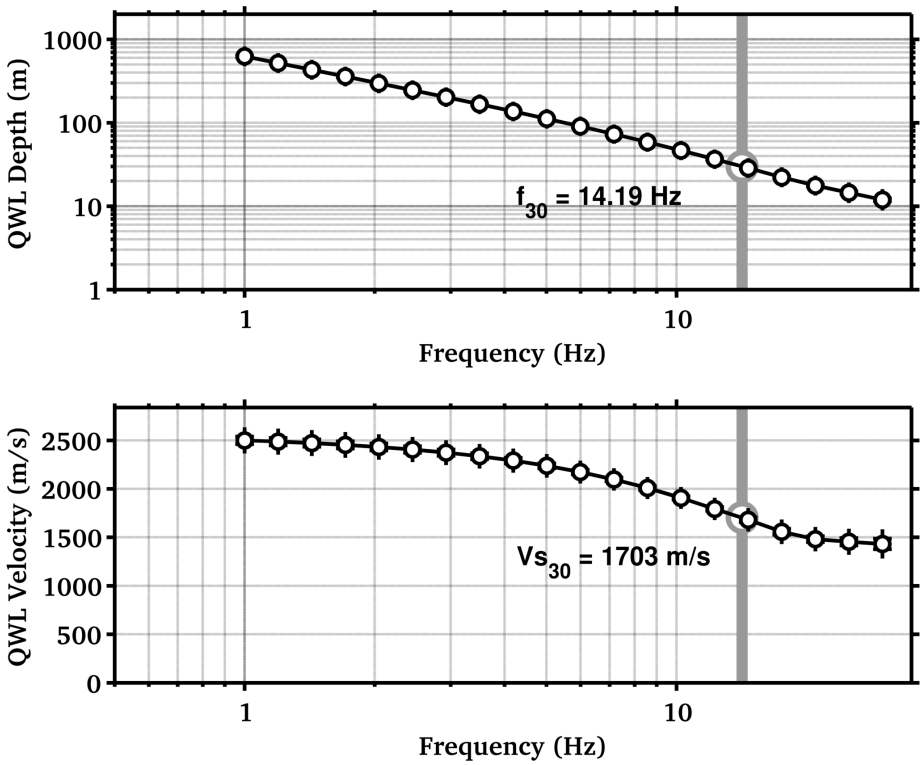

Figure 20 - *Quarter-wavelength representation of the inverted S-wave velocity profiles. Top: the depth-frequency dependency. Bottom: the QWL average velocity. The Vs30 value is indicated with its corresponding QWL frequency.*

12. Amplification models

Site amplification functions have been computed using two different approaches: the S-wave transfer function for vertical propagation and the quarter-wavelength amplification. In general the first method is used to evaluate the resonance characteristics of the site, while the second is more useful to assess the effect of the velocity contrasts between the lowermost rock layer (as reference) and the different QWL averaging depths. The two amplification functions are then corrected for the Swiss rock reference velocity profile as defined in Poggi et al. (2011), according to the procedure described in Edwards et al. (2013). Given the lower velocities in the uppermost part of the BERGE profile compared to the Swiss reference, the final corrected amplification function results in a general deamplification, with an average factor of about 0.3 at high frequencies (Figure 21).

Averaging depth	Vs-mean (m/s)	S.D.
5	1356.45	111.79
10	1416.48	61.66
15	1459.69	31.99
20	1514.80	22.54
25	1614.01	20.36
30	1703.22	15.88
40	1833.41	14.31
50	1939.84	12.86
75	2106.16	16.01
100	2204.53	20.20
150	2313.10	26.13
200	2371.50	29.69

Table 1 - *Average travel time velocities at different depths. Vs30 is highlighted.*

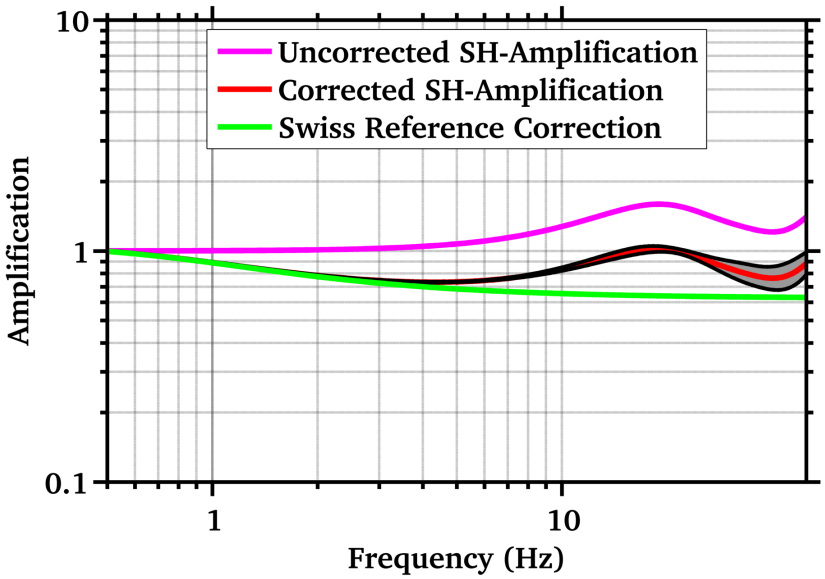

Figure 21 - *Correcting the SH-wave transfer function for the Swiss (rock) reference conditions (Poggi et al. 2011). The final corrected function shows a clear (average) deamplification of about 0.3 at high frequencies.*

Amplification functions using the transfer function and the quarter-wavelength approach are comparable (**Figure 22**), even if the transfer function provides a slightly larger amplification, because of the presence of some weak resonance peaks. At low frequencies both methods converge to the same amplification level. It has to be notice that the amplification functions do not include attenuation at this stage of the analysis, as the quality factors of the site are unknown.

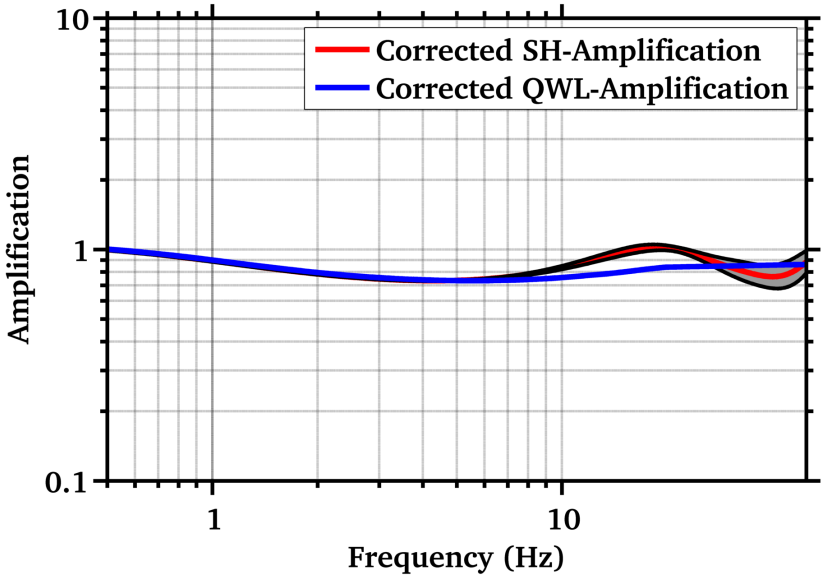

Figure 22 - *Comparison of amplification functions computed using the SH-wave transfer function and the quarter-wavelength formalism on the inverted velocity models. The functions are referenced to the Swiss rock reference model (Poggi et al. 2011).*

REFERENCES

Capon, J., 1969. High resolution frequency wavenumber spectrum analysis, Proc. IEEE, 57, 1408-1418.

Burjanek, J., G. Stamm, V. Poggi, J.R. Moore, and D. Fäh [2010], "Ambient vibration analysis of an unstable mountain slope", Geophys. J. Int., Vol. 180, pp. 820-828.

Edwards, B., C. Michel, V. Poggi and D. Fäh (2013). Determination of Site Amplification from Regional Seismicity: Application to the Swiss National Seismic Networks. Accepted for publication in Seismological Research Letters.

Joyner, W. B., R. E. Warrick and T. E. Fumal (1981). The Effect of Quaternary Alluvium on Strong Ground Motion in the Coyote Lake, California, Earthquake of 1979, Bulletin of the Seismological Society of America, 71, 1333-1349.

Poggi, V., B. Edwards and D. Fäh (2011). Derivation of a Reference Shear-Wave Velocity Model from Empirical Site Amplification, Bulletin of the Seismological Society of America, 101, 258-274.

Poggi, V. and Fäh D., 2010. Estimating Rayleigh wave particle motion from three-component array analysis of ambient vibrations. Geophys. J. Int., 180-1, 251-267.

Huguet. F. (2007). Cirques glaciaires et étagement des formes dans le massif du Feldberg, dans le sud de la Forêt Noire (Allemagne). Géomorphologie: relief, processus, environnement. 4, 309-318.